BIOFLUID ACTIVATED MICROBATTERY FOR DISPOSABLE MICROSYSTEMS

By

EDGAR FELIPE GARAY

A THESIS PRESENTED TO THE GRADUATE SCHOOL
OF THE UNIVERSITY OF FLORIDA IN PARTIAL FULFILLMENT
OF THE REQUIREMENTS FOR THE DEGREE OF
MASTER OF SCIENCE

UNIVERSITY OF FLORIDA

2013

To my mother, for all her love and support

ACKNOWLEDGMENTS

I would like to thank my mother, Irene, family, professors, and friends who have provided me with the emotional support and valuable advice that has helped me during the Master's program. I am grateful for the example my mother has always set for me by working hard every day. I also want to thank Irene for his love and support. In addition, I want to express my gratitude towards my mentor, Dr. Rizwan Bashirullah, for nurturing my enthusiasm for science.

TABLE OF CONTENTS

page

ACKNOWLEDGMENTS 4

LIST OF TABLES 6

LIST OF FIGURES 7

LIST OF ABBREVIATIONS 8

ABSTRACT 9

CHAPTER

1 MOTIVATION 10

2 BATTERY THEORY 12

Battery Performance Metrics: 13
Batteries at the Microscale 15
On-Demand Microbatteries 15
Additional Microbattery Systems 18

3 SILVER OXIDE ALUMINUM BATTERY 22

Usage Model 22
Al-AgO Battery Chemistry 23
Battery Design and Fabrication 24
Fabrication Process Flow 25
Cathode and Anode Fabrication 28
Microbattery Release 30

4 RESULTS AND DISCUSSION 33

Microbattery Structure and Composition 33
Electrical Characterization 33
Sodium Hydroxide Electrolyte 35
Microbattery Activated by Biofluids 40
Conclusions 45

LIST OF REFERENCES 47

BIOGRAPHICAL SKETCH 50

LIST OF TABLES

Table		page
2-1	Electrochemical equivalents of common anode and cathode materials	16
3-1	Microbattery sizes with their respective naming convention	26
3-2	Different methods for depositing Silver Oxide and their measured open circuit voltage	29
4-1	Electrical performance comparison for microbatteries activated using NaOH.	39
4-2	Electrical performance of microbatteries as a function of area and volume	39
4-3	Capacity of microbatteries activated using physiological fluids	40
4-4	Electrical performance of microbatteries activated using physiological fluids as a function of area and volume.	40
4-5	Performance comparison between our microbatteries and previously published microbatteries	44

LIST OF FIGURES

Figure		page
2-1	Battery schematic and operation	12
2-2	Ragone plot showing electrical performance of conventional battery technologies and the best previously published microbatteries. This plot was adapted from Pikul *et al.* [28]	20
3-1	Microbattery usage model where the analyte is used to activate the battery	23
3-2	Flexible microbattery electrode geometry and cross sectional views of the microbattery	25
3-3	Fabrication process of the microbattery.	27
3-4	Two different methods used to deposit silver oxide	29
3-5	Microbattery dicing and release by plasma etching Si substrate	31
3-6	Microbattery images..	31
3-7	Microbattery electrodes on a polyimide substrate attached to a gelatin capsule. Photo courtesy of Edgar Garay.	32
4-1	XEDS spectrum and SEM micrographs.	34
4-2	Experimental output voltage for microbatteries	36
4-3	Microbattery experimental efficiency.	37
4-4	Voltage output for microbatteries activated using different electrolytes	41
4-5	Voltage output for microbattery type S60 and S45 activated using blood	42
4-6	Ragone plot comparing the performance of our microbattery with previously published batteries and commercial technologies	43

LIST OF ABBREVIATIONS

Al	Aluminum
AgO	Silver Oxide
CMOS	Complementary metal oxide semiconductor
Cu	Copper
IC	Integrated circuit
l	Electrode length
LOC	Lab on a chip
MEMS	Microelectromechanical systems
OH	Hydroxide
PI	Polyimide
PR	Photoresist
RF	Radio frequency
s	Electrode spacing
Si	Silicon
SiN	Silicon Nitride
Ti	Titanium
w	Electrode width

Abstract of Thesis Presented to the Graduate School
of the University of Florida in Partial Fulfillment of the
Requirements for the Degree of Master of Science

BIOFLUID ACTIVATED MICROBATTERY FOR DISPOSABLE MICROSYSTEMS

By

Edgar Felipe Garay

December 2013

Chair: Rizwan Bashirullah
Major: Electrical and Computer Engineering

A flexible microbattery activated by blood, urine, saliva, or aqueous sodium hydroxide for disposable medical and biological microsystems is presented. We developed a new CMOS compatible process in order to fabricate a microbattery on a flexible polyimide substrate using conventional MEMS techniques. The microbattery has interdigitated electrode geometry and uses aluminum as the anode, silver oxide as the cathode, and copper as the current collectors. Four different silver oxidation methods were explored to optimize battery performance. The proposed microbattery has a minimum footprint area of 12 mm^2 and is activated by micropipetting 8 µL of the activation fluid onto the surface of the battery. Seven different batteries having different electrode width and spacing were fabricated and characterized. The experimental results show a maximum voltage output of 1.75 V, current output of 0.55 mA, capacity of 7.17 µAh, and a maximum operating time of 75 minutes.

CHAPTER1
MOTIVATION

The continued trend towards CMOS scaling has allowed integrated circuit (IC) designers to implement complex ultra-low power systems that can be turned on using only a fraction of a volt [1-4]. The recognition that such low power systems are capable of gathering, analyzing, and transmitting data has fueled the search for new disposable devices, such as electronic RFID tagging devices for medication compliance, lab-on-a-chip (LOC) for health screening, and food sensors, among others [5-8]. As a result, batteries at the micro scale are becoming more adequate as power sources for these devices. Unfortunately, battery manufacturers still employ manufacturing techniques that are not capable of delivering disposable and biocompatible power sources with a small enough form factor that could be integrated with the before mentioned microsystems. Many of the research efforts have been directed towards the utilization of semiconductor device fabrication technology to develop batteries at the micro scale [9-13]. A variety of microbattery architectures have been proposed ranging from complex 3-dimensional structures to ink jet printed batteries [14-17], but many obstacles are still impeding their implementation into microsystems. The proposed microbatteries employ intricate microfabrication schemes that involve the injection and encapsulation of the electrolyte, which hinders the possibility of mass producing them at a low cost [11, 18]. In addition to the small energy content, batteries using corrosive electrolyte suffer from a high self-discharge rate that translates into a short battery shelf life. For batteries using solid electrolyte, the high temperature steps in the manufacturing process renders the fabrication incompatible with conventional IC fabrication [19, 20]. Disposable microbatteries that have been proposed in the past employ a difficult stacking of

multiple layers in order to separate the electrodes to make room for the electrolyte to flow [21]. Biofluid activated batteries using water and urine as the activation fluid and having a footprint area of 24 cm^2 have also been demonstrated in the past [22-25]. The large footprint area of the battery and the plastic lamination technology used for fabrication do not make it a viable solution as a power source for medical and biological microsystems. There is a current need for a low cost, flexible, on demand, and biocompatible battery that could be easily integrated with low power medical and biological microsystems. This work presents a concept for a disposable, flexible and conformal paper-like microbattery to enable new modes of use of inexpensive biosensors in point-of-care settings.

CHAPTER 2
BATTERY THEORY

A battery is a system composed of one or more electrochemical cells that convert the chemical energy stored in its active components into electric energy. These types of cells are known as galvanic cells and perform energy conversion through an electrochemical oxidation-reduction process, also known as a redox reaction. In the case of a rechargeable cell, this reaction occurs in two directions for charging and discharging. There are three major components in a cell: anode or negative electrode, cathode or positive electrode, and electrolyte. When the anode and cathode are connected through an external load, the anode is spontaneously oxidized in the presence of the electrolyte and gives up electrons to the external circuit. The anode accepts these electrons from the external circuit as it is being reduced. The electrolyte is responsible for providing the conductive medium for the ionic charge transfer between positive and negative electrode. The schematics of a conventional battery are shown in Figure 2-1.

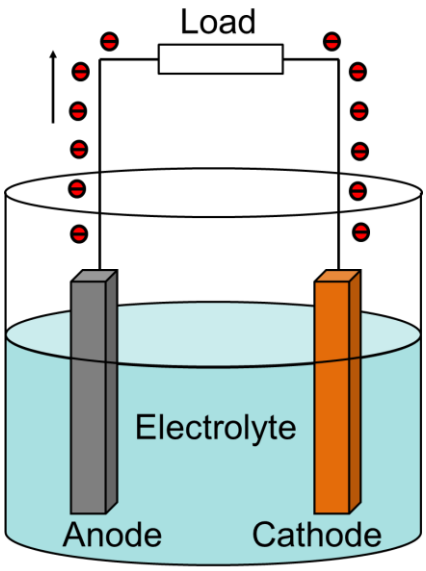

Figure 2-1. Battery schematic and operation.

Batteries are classified according to their electrical capabilities as primary and secondary batteries. Additionally, batteries are also classified depending on their usage model and design. In primary batteries, the electrochemical reaction is not reversible or cannot be effectively reversed, therefore once fully discharge they have to be thrown away. Primary cells are often used in a variety of consumer electronic products where a long shelf life and high energy density at low discharge rates are needed. On the other hand, rechargeable or secondary batteries can be restored to their original condition by supplying a current through their terminals in the opposite direction of the discharge current. The energy density and capacity retention is usually lower than in primary batteries, but their ability to be charge and discharge at high current rates make them ideal for portable electronics. Within primary batteries, reserve batteries are a type of unrechargeable cells in which a main component of the battery is added moments prior to operation. Cells that employ high energy density materials suffer from a high rate of self-discharge, which hinders their implementation in real systems. In this type of batteries, liquid electrolyte is the component added prior to operation in order to obtain long storage periods without depleting the stored energy by self-discharge. Reserve batteries are used in systems that require extremely high power and long storage periods, such as torpedoes, missiles, and other underwater military applications.

Battery Performance Metrics:

Experimental battery performance depends on the chemistry of the cell, and varies from the theoretical performance depending on the efficiency. The theoretical voltage (V) of the cell or standard potential is calculated form the free energy data under standard conditions. The experimental output voltage of the cell during discharge will depend on the discharge conditions and usually varies depending on the battery state of

charge. Depending on the chemistry, some batteries will discharge at a constant voltage while others will gradually decrease their output voltage until fully discharged. Overpotentials in a galvanic cell can also lower the maximum experimental voltage obtained. Batteries are also characterized in terms of capacity. For a battery, capacity is the amount of charges that can be extracted or stored and is commonly reported in amperes-hour (Ah) or Coulomb (C). In the case of a resistance static measurement the experimental capacity can be found using the following equation:

$$C_{exp} = \int i(t)\, dt \tag{2-1}$$

where i is the current drawn from the battery in A and C_{exp} is the battery capacity in Ah. The amount of energy extracted from the battery is another useful parameter used to characterize battery performance. Energy is usually reported as watt-hour (Wh) or joules (J) and can be found using the following equation:

$$E_{exp} = \int v(t) \times i(t) dt \tag{2-2}$$

where v is the output voltage in V and i is the output current in A. Additionally, the maximum power (W) that the battery can output can be obtained:

$$P_{max} = v_{max} \times i_{max} \tag{2-3}$$

where v_{max} and i_{max} are the maximum voltage and current drawn from the battery. From these values efficiency can also be calculated by comparing experimental and theoretical values. It is customary to normalize these quantities by weight and volume in order to compare performance among batteries. In industry, batteries are characterized by fully discharging the battery in a period of 20 hours at a constant current. The capacity of the battery is then calculated by multiplying 20 hours times the current and is reported in mAh. The discharge current is then label C/20; here C stands for capacity

and not for coulombs. For example, if the battery was discharged at a constant current of 200mA, then the capacity would be 4000mAh for a C/20 rate. It should be pointed out that if the battery is discharge at a rate of 1C, the discharge time most likely would be close to 40 minutes and not 1 hour. This is due to the Peukert effect which lowers the capacity when discharging at higher current densities. For batteries at the microscale is useful to normalize by the footprint area in cm^2 and battery thickness in μm. Therefore, units are $\mu Ah/cm^2\mu m$ for capacity, $\mu Wh/cm^2\mu m$ for energy density, and $mW/cm^2\mu m$ for power density.

Batteries at the Microscale

Over the past decades, low power wireless links have opened the doors for a new array of microsystems that are able to gather and transmit data while consuming an average power of less than 100 μW [3]. These improvements are the driving force behind the research focused on finding new materials and battery geometries at the microscale that will help create a battery that delivers enough energy and power to miniaturized wireless nodes. Microbatteries can be categorized into thin film, thick film, solid state, printed, three dimensional, and on-demand microbatteries. Commercial realization of microbatteries is not possible yet, since device performance is still far from optimal. Additionally, concerns regarding scalability, stability, and fabrication costs still need to be addressed.

On-Demand Microbatteries

Among new microbattery designs, an innovative battery type has emerged that utilizes biofluids as the activation electrolyte for on-demand use. These microbatteries employ the same usage model as reserve batteries, in which the

electrolyte is added to the battery moments prior to use. On-demand microbatteries can potentially provide enough power and energy for lab-on-a-chip applications, food sensors, medical implants, and many other biomedical applications. In the case of lab-on-a-chip applications, the microbattery would use the test liquid as the electrolyte to convert the stored chemical energy into electrical energy. Depending on the battery chemistry, physiological fluids, such as blood, urine, and saliva could also be used as the electrolyte. One of the main advantages of on-demand microbatteries is that highly active materials can be implemented in a small foot print to obtain sufficient energy without suffering from high self-discharge rates. Table 2-1 shows the theoretical capacity of different materials. As an example, Al and AgO are two of the materials with the highest capacity density, but it is difficult to implement them in real battery systems due to their instability and high self-discharge rate.

Table 2-1. Electrochemical equivalents of common anode and cathode materials.

Material	**Standard potential (V)**	**Ah/g**	**Ah/cm³**
	Anode Material		
Li	-3.01	3.86	2.06
Mg	-2.38	2.20	3.80
Al	-1.66	2.98	8.10
Ca	-2.84	1.34	2.06
Fe	-0.44	0.96	7.50
Zn	-1.25	0.82	5.80
Pb	-0.13	0.26	2.90
$(Li)C_6$	-2.80	0.37	0.84
	Cathode Material		
O_2	1.23	3.35	-
MnO_2	1.26	0.31	1.54
NiOOH	0.49	0.29	2.16
CuCl	0.14	0.27	0.95
AgO	0.57	0.43	3.20
Ag_2O	0.35	0.23	1.64
Li_xCoO_2	2.70	0.14	-

On-demand microbatteries using sulfuric acid and hydrogen peroxide as the electrolyte have been previously developed [21]. This battery employs gold and zinc as the electrodes and silicon as the substrate. The battery was fabricated using conventional MEMS techniques for depositing and patterning the gold electrode and the cathode and anode separator. The fabrication is completed by manually bonding a thick (~1 mm) piece of zinc on top of the battery. The total area of the battery was 1 mm^2 and exhibits a maximum energy density of 204 µWh cm^{-2} and a maximum output voltage of 1.5 V under a 10 kΩ load. The highly corrosive electrolyte prevents the safe integration of this battery into biomedical microsystem.

Sammoura *et al.* fabricated a water-activated microbattery for BioMEMS chips by using a one mask MEMS process [25]. This battery prototype used a 15 µm thick magnesium anode and a 20 µm thick AgCl cathode. The two electrodes are deposited into a silicon substrate and are bonded together using and adhesive, which also serves as a separator. The electrode separation ranged from 50 to 200 µm. A battery with a 1.44 cm^2 electrode area exhibited a maximum output voltage of 1.65 V and a maximum energy capacity of 1.8 mWh. The authors also demonstrated that decreasing the gap between anode and cathode can improve the efficiency of the battery.

The first on-demand paper battery activated by urine was previously demonstrated by Lee [22]. The battery used Cu and Mg electrodes and a CuCl-doped filter paper. This battery was fabricated using an inexpensive plastic lamination process in which thick (~0.2 mm) sheets of Mg, Cu, Al, filter paper, and plastic film are stacked together to form the battery. The total area of the battery is 18 cm^2 and is able to provide a maximum power output of 1.5 mW. A second prototype for this battery was

developed where the battery was activated using urine, water, and saliva [23]. The battery had an area of 24 cm^2 and it was fabricated using the same chemistry and lamination technology. The battery exhibited a maximum output voltage of 1.56 V that decreased over time and a maximum power output of 15.6 mW.

Another example of an on-demand and biocompatible battery was proposed by Jimbo and Miki in which the gastric fluid in the stomach was used as the activation electrolyte [24]. This battery consists of a Pt and Zn electrodes on a glass substrate, a porous ceramic filter, and a PDMS case. The fabrication process consisted on sandwiching the ceramic filter in between the electrodes and the using a PDMS to case to hold them together. The battery had a total area of 120 mm^2 and a thickness of 4 mm. This battery was able to generate a stable 0.6 V for 40 min with a 5 kΩ load resistor. The maximum energy capacity achieved was 0.1 mWh when using a 500 Ω load resistor, which translates into an energy density of 0.021 $\mu Wh\ cm^{-2}\mu m^{-1}$.

Additional Microbattery Systems

The first 3-D rechargeable Lithium-ion thin-film microbattery was developed in 2005 by Nathan *et al.* [10]. This microbattery used a perforated silicon substrate with through-holes formed by plasma etching. The fabrication of the battery consisted of different electroplating steps and the preparation and spin coating of a slurry to fill the cylindrical cavities of the battery. The microbattery had a disc-like form factor with a diameter of 13 mm and a thickness of 0.5 mm. The output voltage ranged from 2.2 to 1.2 V maximum and the microbattery displayed a capacity of 2 $mAh\ cm^{-2}$. Additional 3-D microbattery architectures have been developed in the past in which silicon micromachining techniques and electroplating are utilized to fabricate them. Chamran *et al.* developed a Ni-Zn rechargeable microbattery using interdigitated electrode arrays

composed of high aspect ratio microscale posts [11]. The results indicated that the battery could only be used for a few cycles due to the etching of the electrodes by the electrolyte.

A different approach to 3-D microbatteries was taken by Min *et al.* in which the used a carbon-microelectromechanical systems (C-MEMS) microfabrication process to fabricated a Li-ion battery [26]. The battery consisted of arrays of carbon posts interdigitated with arrays of dodecylbenzenesulfonate-doped polypyrrole and a 1 M $LiClO_4$ electrolyte. The battery prototype demonstrated that it could function as a secondary battery with an areal capacity of 10.6 μAh cm^{-2}. On the other hand, the battery exhibited a short life of only 12 recharging cycles due to an internal short.

An all-solid-state Li ion battery employing a honeycomb pattern was previously developed by Kotobuki *et al.* [27]. The authors studied the properties of the interface between the solid electrodes and solid electrolyte. The output voltage of the battery was 1.2 V and a discharge capacity of 32 μAh cm^{-2}. A different solid-state lithium microbattery was developed by Song *et al.* using a microfabrication process [19]. The area of a single microbattery was 500 μm x 500 μm and its thickness was 1.5 μm. The fabrication included a high temperature step of 500 °C. The battery delivered a maximum capacity of 17 nAh and could be discharged at a maximum current of 40 nA.

The need for smaller batteries with a high energy density has motivated the development of additional methods for fabricating batteries. Ho *et al.* developed a direct write dispenser printing method to fabricate a Zn and MnO_2 microbattery with an ionic

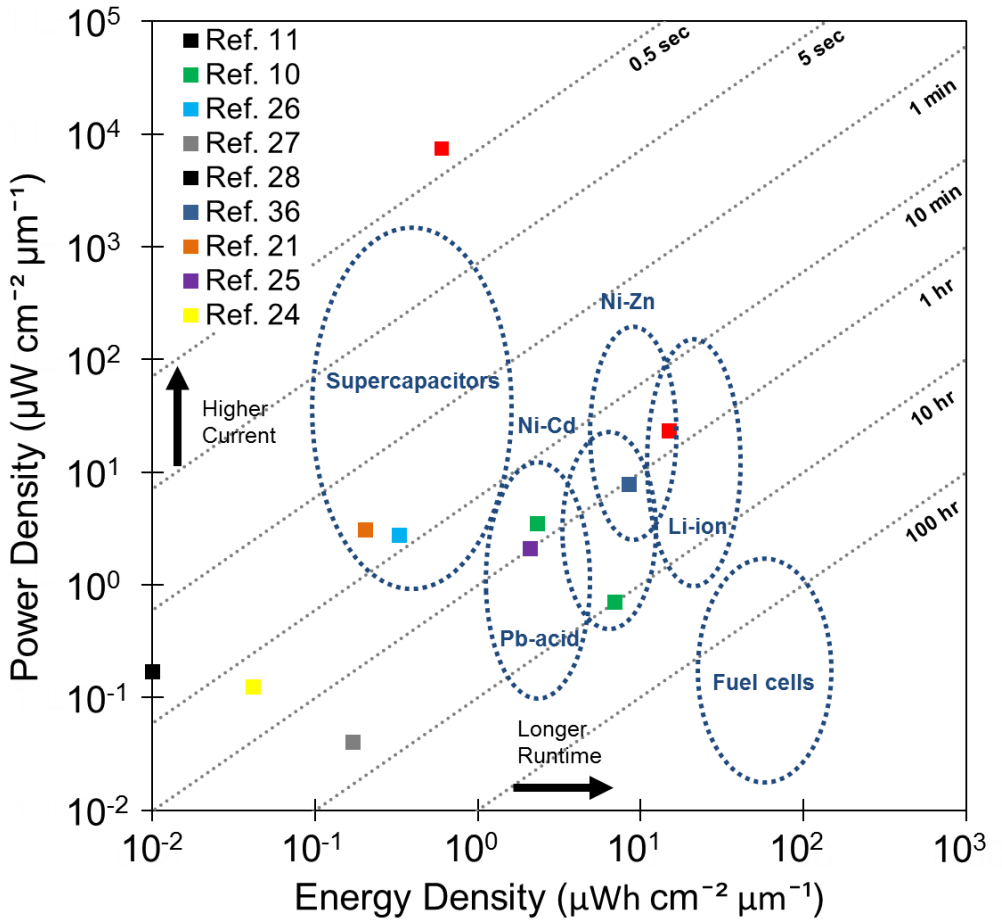

Figure 2-2. Ragone plot showing electrical performance of conventional battery technologies and the best previously published microbatteries. This plot was adapted from Pikul *et al.* [28].

liquid gel electrolyte. Their first experiments showed that the battery had a capacity of 0.98 mAh cm^{-2} for more than 70 cycles. A different method for depositing thick-film electrodes employs a laser direct-write technique [29]. In this method, a laser pulse is used to transfer ink or paste onto a substrate. Thick film microbatteries using this method exhibited a capacity of 2500 μAh cm^{-2}. Thick-film microbatteries have a higher areal capacity than thin-film microbatteries due to their large volume.

Recently, Pikul *et al.* developed a high performance 3-D lithium ion microbattery having a power density greater than that of super capacitors [28]. The

battery consisted of interdigitated electrodes in which a porous metallic scaffold was used to electroplate the active materials. The microbattery used a 1 M $LiClO_4$ liquid electrolyte and a silicone cover to hold the liquid. The total volume of the cell was about 0.3 mm^3 and it showed energy densities form 2.5 to 15 $\mu Wh\ cm^{-2}\ \mu^{-1}$ and a maximum power density of 7400 15 $\mu W\ cm^{-2}\ \mu^{-1}$. This is equivalent to 2000 times the power density of the best microbatteries in literature and larger energy density than batteries in previously published work. The performance comparison of conventional battery technologies and best performing published microbatteries is shown in Figure 2-2.

CHAPTER 3
SILVER OXIDE ALUMINUM BATTERY

Usage Model

We designed the microbattery as a disposable and on-site activated battery on a flexible polyimide platform for lab-on-a-chip applications. This microbattery exploits the chemical reactivity of the analyte being tested by using it as an electrolyte in order to convert the stored chemical energy of the microbattery into electrical energy. This simple approach avoids the need for fabricating a sealed container and injecting the electrolyte. Additionally, the self-discharge due to the parasitic corrosion of the electrodes when the electrolyte is present is eliminated. Furthermore, the microbattery can be activated with a range of different biofluids, such as blood, urine, saliva, water, milk, and any other aqueous solution containing the hydroxide ion. Figure 3-1 shows the intended usage model for the microbattery.

Three different criteria were applied when designing the microbattery: ease of fabrication, CMOS compatibility, and minimization of the battery internal resistance. For the microbattery fabrication, we utilized a CMOS compatible MEMS manufacturing technology [30]. The simple fabrication steps and low temperature process developed for this work, allows for an easy scalability to volume manufacturing and integration with CMOS ICs. Moreover, the ability to implement different designs within the same mask allows for the manufacturing of microbatteries having different capacities, thus permitting the fabrication of microbatteries for different applications within the same wafer.

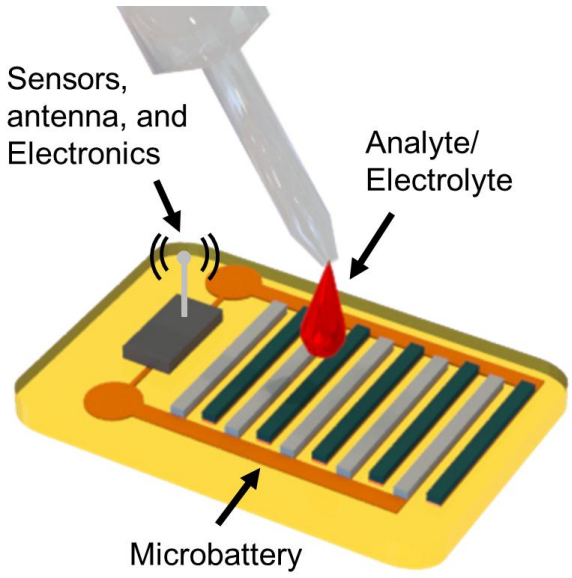

Figure 3-1. Microbattery usage model where the analyte is used to activate the battery.

Al-AgO Battery Chemistry

The microbatteries in this work use aluminum (Al) as the anode and silver oxide (AgO) as the cathode. Large scale batteries based on aluminum-silver oxide have found use as power sources in military underwater applications due to their high energy density and prolonged storage periods [31]. Al was chosen as the anode due to its electrochemical properties, easy of fabrication and potential use as a biocompatible material. This type of batteries uses an alkaline solution as the electrolyte, making the hydroxide ion the responsible for the conduction inside the battery. The major chemical reactions for the oxidation at the anode and the reduction at the cathode are given by Equation 3-1 and Equation 3-2 [31-33]:

$$Al + 4OH^- \rightarrow Al(OH)_4^- + 3e^- \quad (3\text{-}1)$$

$$AgO + H_2O + 2e^- \rightarrow Ag + 2OH^- \quad (3\text{-}2)$$

and the overall cell reaction is given by:

$$2Al + 3AgO + 2OH^- + 3H_2O \rightarrow 2AlOH_4^- + 3Ag \quad (3\text{-}3)$$

The standard potential of this cell is obtained from the free-energy data under standard conditions. Depending on the oxidation state of the silver the theoretical open circuit cell voltage ranges from 2.695 to 2.952 V. However, batteries using aluminum as the anode material tend to operate at a lower potential due to the parasitic corrosion of the aluminum and because at room temperature aluminum forms an oxide layer that increases the internal resistance of the battery [34].

Battery Design and Fabrication

The microbattery consists of a series of interdigitated electrodes that alternate between anode and cathode. We chose this battery geometry to minimize the internal resistance of the battery, maximize the surface area, and to avoid complicated fabrication schemes that ultimately will hinder the scalability of the microbatteries to large volume manufacturing. In addition, the interdigitated electrodes allow for the battery to be flexed without delamination of the metal layers due to the stresses caused by the bending of the battery. Current collectors for the anode and cathode were fabricated from copper (Cu) in order to offset the increase of internal resistance during the operation of the battery due to the low conductivity of the silver oxide and the aluminum depletion. Silicon nitride was used as the insulating layer to avoid short circuiting the anode and the cathode current collectors when the liquid electrolyte is present.

Seven microbattery designs having different electrode finger widths (w) and electrode spacing (s) were fabricated. The batteries dimensions are shown in Figure 3-2 and Table 3-1 summarizes the different microbattery geometries and the naming convention used in this paper for each microbattery. The fabrication of the microbatteries was carried out in a class 100-1000 cleanroom facility. All metals were

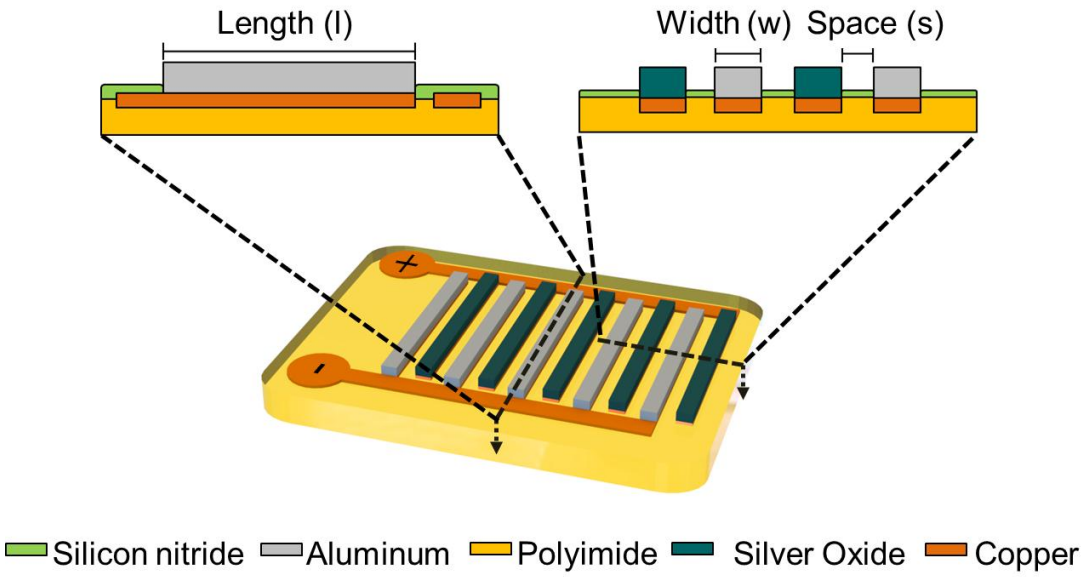

Figure 3-2. Flexible microbattery electrode geometry and cross sectional views of the microbattery.

deposited using a KJL CMS-18 sputtering deposition system. All the UV lithography steps were performed using the EVG 620 mask aligner.

Fabrication Process Flow

The process flow for the fabrication of the microbattery is depicted in Figure 3-3. A 100 mm mechanical grade silicon wafer was used as the carrier wafer for the entire fabrication process. The silicon wafer was cleaned by dipping the wafer in hydrofluoric acid for 30 seconds and then rinsing it in DI water. The first step as shown in Figure 3-3A was to deposit the polyimide. Polyimide was chosen as the flexible platform for the microbatteries due to its biocompatibility and capability of resisting SiN deposition.VM-652 (HD MicroSystems) was used as the adhesion promoter between the polyimide and the silicon wafer. The VM-652 was dispensed on the static substrate and held for 20 seconds on the wafer. The adhesion promoter was then dried by spinning the wafer at

Table 3-1. Microbattery sizes with their respective naming convention.

Battery type	Width (μm)	Space (μm)	Length (mm)	Electrode Area (mm^2)	Mass Al (μg)	Mass AgO (μg)	Footprint area (mm^2)
WS30	30	30	2.6	3.26	8.80	36.58	12.64
W45	30	45	2.6	3.26	8.80	36.58	15.82
W60	30	60	2.6	3.26	8.80	36.58	18.92
W75	30	75	2.6	3.26	8.80	36.58	22.06
S45	45	30	2.6	4.84	13.07	54.30	15.82
S60	60	30	2.6	6.41	17.31	71.92	19.00
S75	75	30	2.6	7.99	21.57	89.65	22.18

4000 rpm for 30 seconds. Following the application of the adhesion promoter polyimide was deposited by spin coating PI-2611(HD MicroSystems). Then, the wafer was soft-baked at 90°C for 120 s followed by 150°C for 90 s. Following the soft-bake, the polyimide was fully cured by baking the wafer at 350°C in a nitrogen atmosphere for 1 hour. The temperature of the oven was gradually increased at 4°C/min from 150° to 350°C. After fully curing the polyimide the oven was turned off and the wafer was left overnight inside the oven allowing the wafer to gradually cool down to room temperature. The final polyimide thickness was roughly 8 μm. After the wafer reached room temperature, a 6 μm thick positive tone photoresist (PR) (AZ 9260, MicroChemicals) layer was patterned using conventional UV lithography. In our fabrication process, we designed the PR layer to serve two different purposes. The PR is first used as the mask to etch the polyimide, and then the same PR layer is used after the polyimide etching to pattern the anode and cathode current collectors. By etching the polyimide and then depositing the collector material using the same mask, the need for planarization steps and a thick SiN layer were avoided. These two steps are described below.

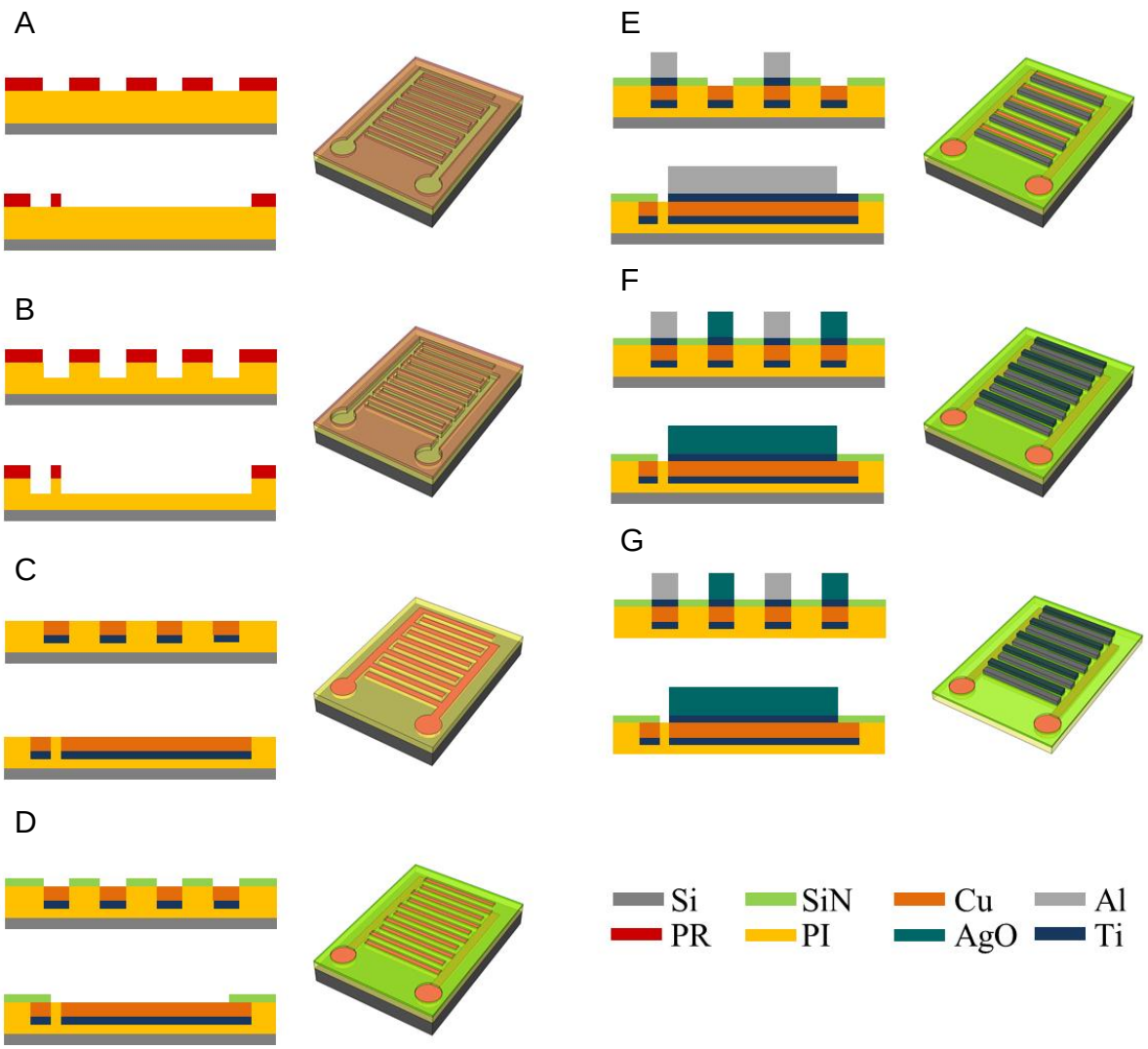

Figure 3-3. Fabrication process of the microbattery. A) spin coat PI, fully cure PI, spin coat and pattern PR. B) dry etch PI. C) Sputter Ti/Cu anode and cathode current collectors and pattern by dissolving PR in acetone. D) Deposit SiN using PECVD, spin coat PR etch mask, dry etch SiN. E) Sputter Al anode, pattern using lift off. F) Deposit AgO using reactive sputtering. G) Release microbattery by etching Si using DRIE.

The polyimide was dry etch using the Unaxis Shuttlelock reactive ion etcher with an inductively coupled plasma module (RIE/ICP) (Figure 3-3B). The process gases for the polyimide etch are O2 and Ar. The etch process follows the recipe developed in [35]. Finding the etch rate of the polyimide was crucial in the fabrication of the

microbatteries. The etch depth had to be the same as the metal thickness of the current collectors so a planar surface could be obtained after the metal deposition.

The current collectors were deposited by sputtering a 100 nm thick Ti adhesion layer followed by a 1 µm thick Cu layer. The collectors were defined by lifting-off the PR in acetone while sonicating for 60 s (Figure 3-3C). After the lift-off process, the metal patterns were inspected using an optical microscope. The optical micrographs indicated poor adhesion between the polyimide and the current collectors. Different approaches were used in order to improve the adhesion. Finally, soft- baking of the wafer at 112°C for 3 min prior to metal deposition greatly improved the adhesion of the metal layers to the polyimide. A 15 min sonication test was used in order to test for proper adhesion.

Current collector patterning was followed by depositing a 100 nm SiN layer using the STS 310PC PECVD system. The nitride layer provided the necessary insulation for the current collectors. The SiN was patterned using PR as the etch mask and dry etched using the Unaxis RIE/ICP (Figure 3-3D). The RF1 power was set to 100 W and the RF2 power was set to 0 W. The process gases were CHF3 and O2 and were set to 27 sccm and 5 sccm, respectively. The chamber pressure was set to 100 mTorr. The SiN etch rate was approximately 125 Å/min.

Cathode and Anode Fabrication

The cathode and anode were sputtered and patterned using conventional lift-off techniques. For the anode, a 100 nm Ti layer was sputtered followed by a 1µm thick Al layer (Figure 3-3E). For the cathode, four different recipes using two different methods for oxidizing Ag were attempted (Figure 3-4). We used the following criteria to select the

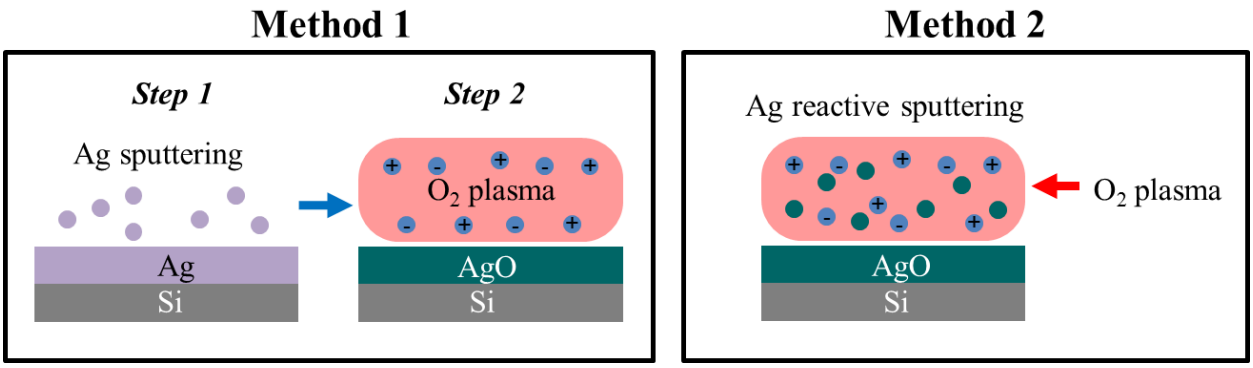

Figure 3-4. Two different methods used to deposit silver oxide.

Table 3-2. Different methods for depositing Silver Oxide and their measured open circuit voltage.

Sample	Oxidation method	Open Circuit Voltage (V)
Sputtered Ag	None	1.71
Recipe 1	Unaxis RIE/ICP O_2 plasma, RF2 = 200 W	2.01
Recipe 2	Unaxis RIE/ICP O_2 plasma, RF2 = 1000W	2.02
Recipe 3	Reactive sputtering, 5% O_2	1.95
Recipe 4	Reactive sputtering, 10% O_2	1.95

appropriate method: ease of fabrication and open circuit voltage. The open circuit voltage between Al and AgO was tested using a 1M aqueous solution of NaOH at room temperature. For all four methods, 1 cm silicon squares were cleaved from a silicon wafer to use as the substrate. Then, a 10 nm Ti adhesion layer was sputtered followed by a 200 nm Ag layer. For the first two recipes, the oxidation of the Ag film was accomplished by exposing the silver layer to oxygen plasma using the Unaxis SLR RIE/ICP. For both recipes, the pressure chamber was kept at 10 mTorr, the oxygen flow was set to 40 sccm, and the RF1 power was fixed at 100 W. The RF2 powers for recipe 1 and 2 were 200 W and 1000 W, respectively. The processing time was 5 min. For

recipes 3 and 4, AgO was directly deposited onto the wafer using reactive sputtering. The percentage of O_2 flow with respect to Ar for recipe 3 and recipe 4 was set to 5% and 10%. Table 3-2 shows the open voltage measurement results for each method.

AgO obtained using recipes 1 and 2 exhibited a higher open voltage potential than AgO directly deposited onto the substrate by reactive sputtering. On the other hand, recipes 1 and 2 displayed a low oxidation depth control and uniformity across the samples. AgO films presented a poor film quality after O_2 plasma oxidation due to the ion bombardment. Since the maximum voltage variation observed from different methods was only 70 mV, ease of fabrication was taken as the most important factor in deciding what process to use; therefore, reactive sputtering was selected as the preferred method for the cathode material deposition since fewer steps are required for the cathode deposition. For the reactive sputtering, recipe 3 and 4 showed the same open circuit voltage. We believe that the maximum oxidation rate was achieved in recipe 3.

For the microbatteries, first a 100 nm thick Ti layer was sputtered and then a 1.5 µm AgO film was deposited using recipe 3. The cathode was then patterned by lift-off, as shown in Figure 3-3F. For these microbatteries, the cathode was deposited thicker than the anode since the depletion rate of the AgO cathode is greater than that of the Al anode. A SEM image of the battery electrodes after anode and cathode deposition is shown in Figure 3-6A.

Microbattery Release

The final step as shown in Figure 3-5 was to release the microbatteries from the Si wafer. First, the microbatteries were diced into individual batteries. Then, the top side of a few (3 to 5) batteries was attached onto a carrier wafer using PR. This allows

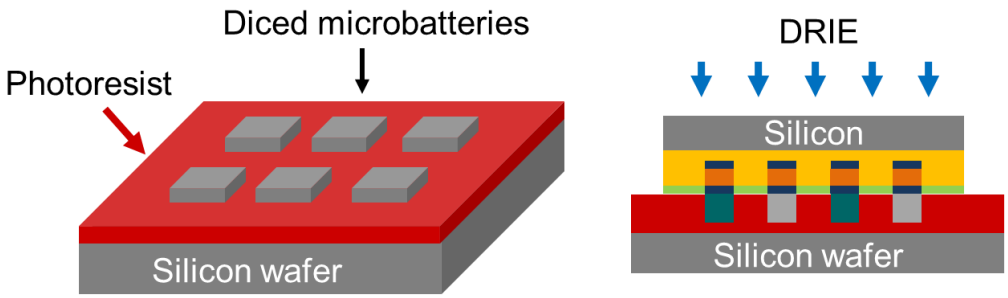

Figure 3-5. Microbattery dicing and release by plasma etching Si substrate.

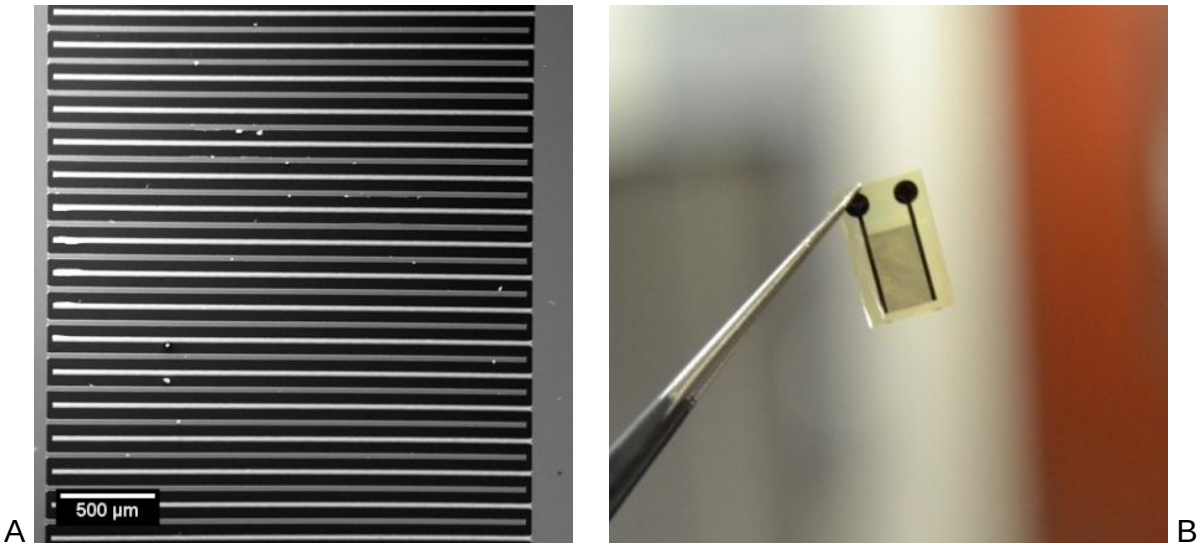

A B

Figure 3-6. Microbattery images. A) SEM image of the microbattery before release. B) photo of the microbattery electrodes on a flexible polyimide substrate. Photos courtesy of Edgar Garay.

etching the Si underneath the microbatteries without exposing the electrodes to the etchants. The carrier wafer with the microbatteries was then placed inside a STS deep reactive ion etching (DRIE) system in order to completely remove the Si (Figure 3-5). The gases for the DRIE process were SF_6 (130 sccm) and O_2 (13 sccm). The 13.56 MHz coil power was set to 600 W and the platen power was set to 12 W. The etching time for the Si had to be carefully controlled since the etchant gases could also attack the polyimide layer. Figure 3-6B shows an image of the microbattery electrodes after

release. As an example of future applications, the microbattery was attached to a gelatin capsule, as shown in Figure 3-7.

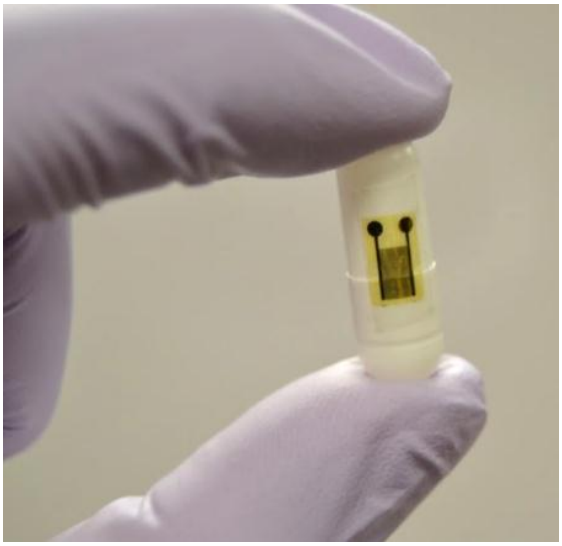

Figure 3-7. Microbattery electrodes on a polyimide substrate attached to a gelatin capsule. Photo courtesy of Edgar Garay.

CHAPTER 4
RESULTS AND DISCUSSION

Microbattery Structure and Composition

The microstructure and composition of the battery anode and cathode were inspected using a FEI Nova NanoSEM 430 field emission scanning electron microscope (SEM). We analyzed the chemical composition by using the energy dispersive x-ray spectroscopy (XEDS) abilities of the SEM. Figure 4-1A shows the XEDS spectrum and microstructure of the Al anode. The main component of the anode is Al, with some traces of Cu, Ti, and Si. These traces are picked up by the x-ray detector since the x-ray spectrum is collected from a volume sample of the anode that contains Cu, Ti, and Si underneath the Al. Figure 4-1B illustrates the cathode x-ray spectrum and the AgO surface morphology. The x-ray spectrum provides evidence of the Ag oxidation using reactive sputtering, as described before. From the SEM image of the anode, the average AgO particle radius is 50 nm. This small grain structure increases the surface area to volume ratio, increasing the reaction surface of the AgO with the electrolyte.

Electrical Characterization

All microbatteries were tested using a resistance-static method by using different resistor values as the load. DC voltage measurements were performed using an Agilent HP 34401A digital multimeter. The digital multimeter was connected to a computer in order to save the data every second using a LabVIEW routine. The microbatteries were activated by micropipetting 8 µL of the target fluid. Aqueous NaOH, blood, urine, and saliva were used as the activation fluid for the experiments. All measurements were performed at room temperature.

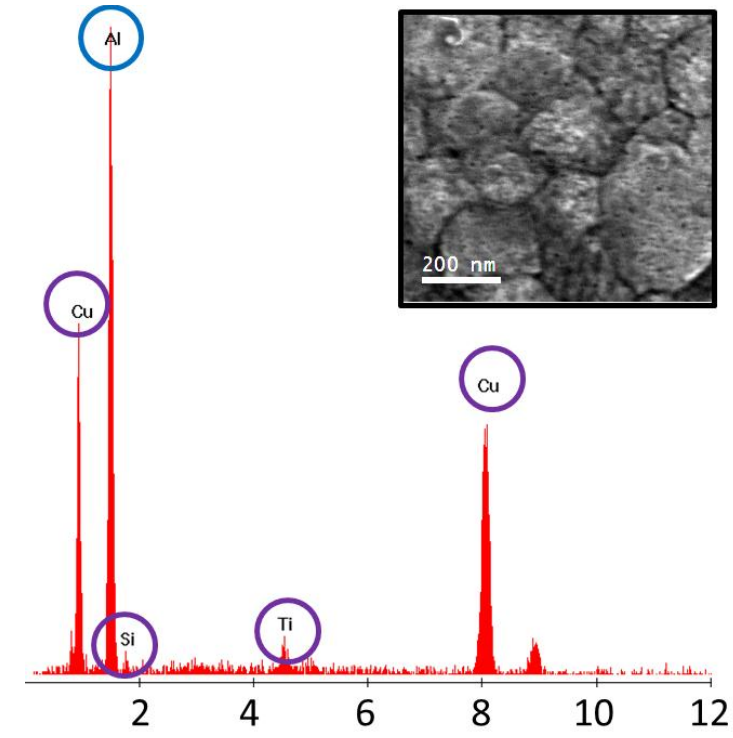

A

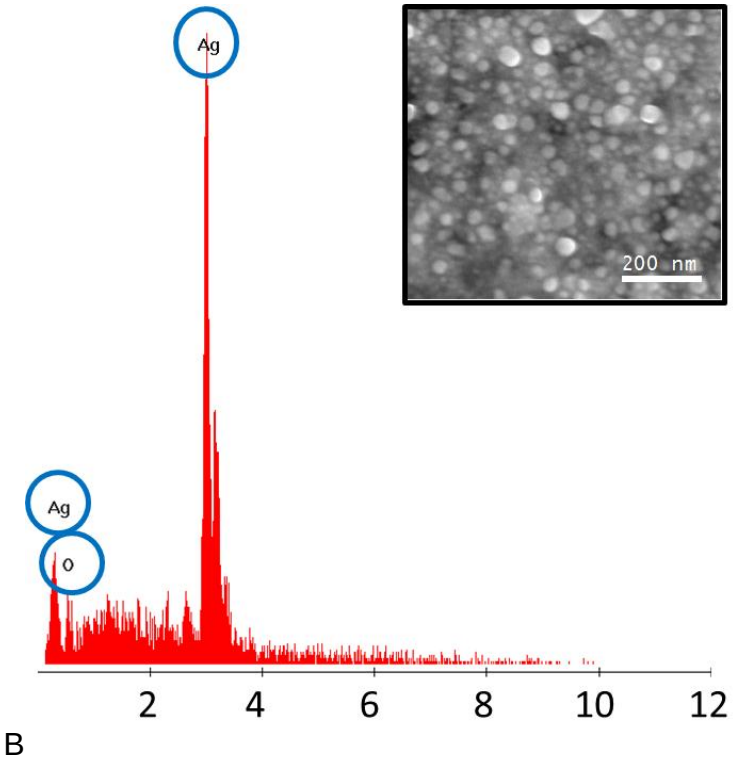

B

Figure 4-1. XEDS spectrum and SEM micrographs. A) Al anode. B) AgO cathode.

Sodium Hydroxide Electrolyte

The output voltage of all 7 microbattery types was initially measured using a 1M aqueous solution of NaOH as the electrolyte and a 100 kΩ resistor as the load. The battery capacity was calculated and analyzed as a function of the electrode finger spacing (batteries S45, S60, and S75) and finger width (batteries W45, W60, AND W75) and compared to the performance of battery SW30, which is taken to be the reference battery. Figure 4-2A shows the preliminary results obtained for the output voltage of SW30 and S45, S60, and S75. The capacity was calculated using Equation 2-1; these results are shown in Table 4-1. The maximum output voltage obtained for the microbatteries activated using NaOH was 1.74 V. We considered 0.2 V as the lower limit of the operational range of the microbattery. From the experimental data obtained, we observed that the microbattery capacity increased as the electrode finger spacing increased. The battery capacity for SW30, S45, S60, and S75 ranged from 1.41 to 5.75 µAh. Decreasing the spacing between fingers from 75 µm to 30 µm has no apparent benefits when discharging the battery at a maximum current density of 0.5 mA/cm2 and maximum load current of 17 µA. We expect that the internal resistance of the microbattery would decrease as the electrode finger spacing is reduced, thus improving the capacity and performance of the microbattery. However, the load current has an important role in the performance of the microbattery. For low load currents, electrode corrosion due to the electrolyte is the main parasitic electrochemical reactions responsible for the lower capacity obtained in our experiments; therefore, capacity evaluation using a 100 kΩ load based on electrode spacing was impossible. Future studies should characterize the current load at which the battery performance becomes a function of electrode finger spacing.

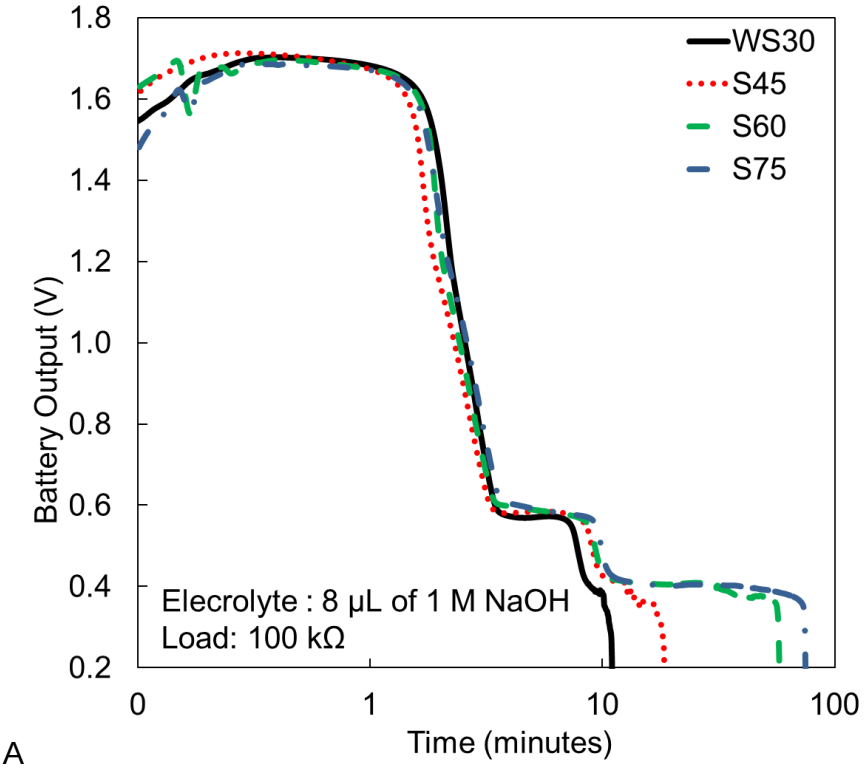

A

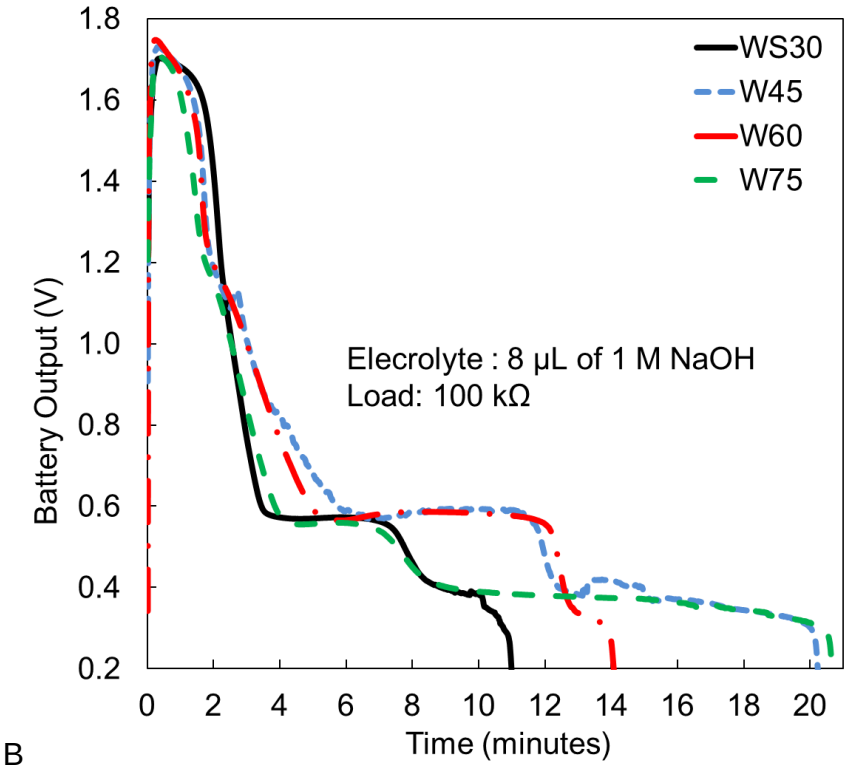

B

Figure 4-2. Experimental output voltage for microbatteries. A) Different electrode fingers spacing. B) Different electrode finger widths.

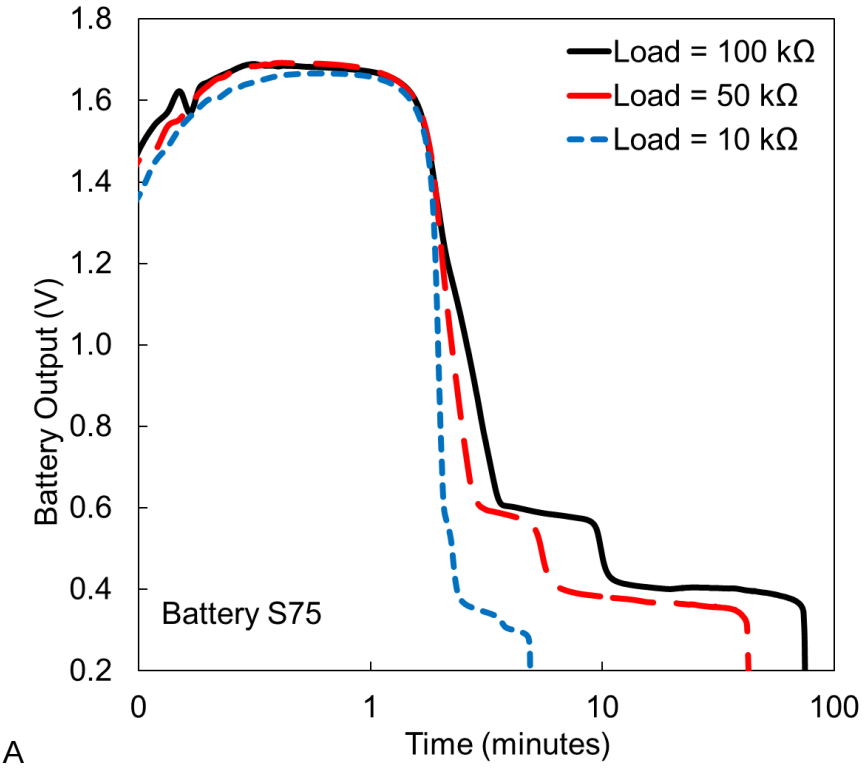

A

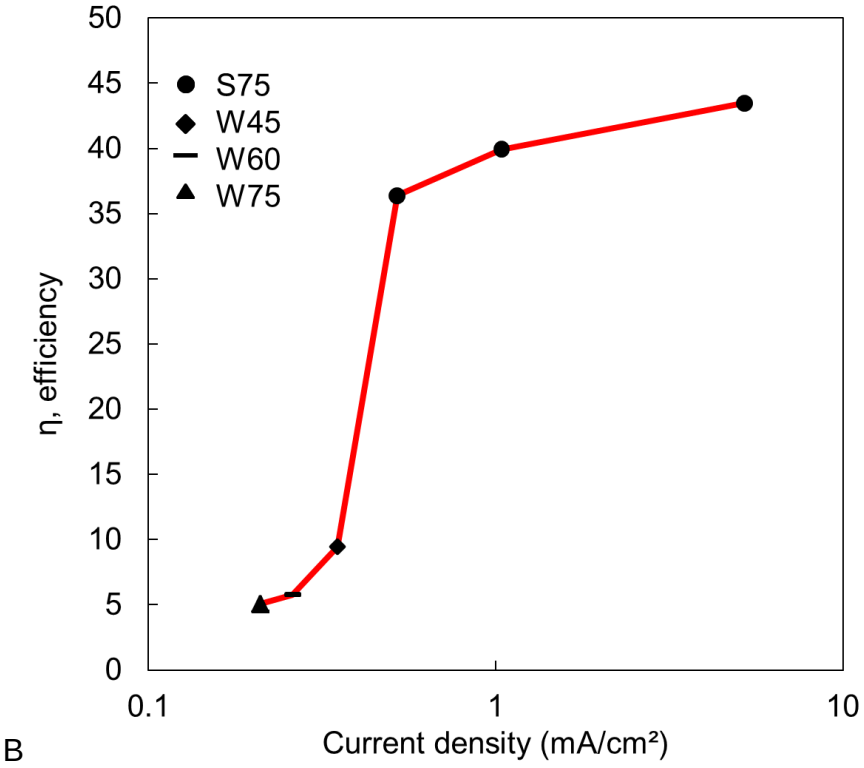

B

Figure 4-3. Microbattery experimental efficiency. A) Voltage output for different loads for battery S75. B) Experimental efficiency as a function of current density.

To validate the importance of the load current in determining battery capacity, the output voltage of battery S75 was also measured for different loads, as show in Figure 4-3A. The capacity for each load is shown in Table 4-1. Initial results show that the experimental capacity increases from 5.75 µAh to 6.87 µAh as the load current is increased from 17 µA to 170 µA. Also, we believe that reducing the electrolyte concentration can dramatically increase the experimental capacity of the microbatteries due to a lower self-discharge rate.

Figure 4-2B illustrates the output voltage measurements obtained for WS30, W45, W60, and W75. From Figure 4-2B, we can see that the output voltage and discharge time are approximately the same. For these microbatteries, the electrode finger width varies from 30 to 75 µm in increments of 15 µm. The width increment of the electrode fingers translates into a larger electrode area, higher theoretical capacity, and lower current density if using a load with the same resistance value. Because we used the same resistor as the load for these experiments, the current density decreases across battery types from battery WS30 to W75, as shown in Table 4-1. The current density was calculated using the drawn electrode area. The efficiency of the microbatteries was also calculated as follows:

$$\eta = \frac{C_e}{C_t} \times 100\% \qquad (4\text{-}1)$$

where C_e and C_t denote the experimental and theoretical capacity, respectively. Figure 4-3B shows the efficiency as a function of the current density for WS30, S75, W45, W60, and W75. From Figure 4-3B, it is observed that the efficiency increases

proportionally to the current density. This relationship between current density and efficiency explains that the experimental capacity for the microbatteries having a larger electrode area is comparable to the capacity of the reference microbattery, which has less than half the electrode area of the largest microbattery (W75) that was fabricated in this work. Table 4-2 shows de electrical performance of the microbatteries per unit volume.

Table 4-1. Electrical performance comparison for microbatteries activated using NaOH.

Battery type	Load (kΩ)	Voltage Range (V)	Load Current (μA)[a]	Current density (mA/cm²)[a]	Theoretical capacity (μAh)	Experimental capacity (μAh)	Energy (μWh)	Power (μW)	η (%)
WS30	100	1.70-0.20	17	0.52	15.80	1.41	1.45	7.94	8.92
S45	100	1.71-0.20	17	0.52	15.80	1.89	1.57	5.12	11.96
S60	100	1.69-0.20	17	0.52	15.80	4.55	2.67	2.77	28.80
S75	100	1.68-0.20	17	0.52	15.80	5.75	3.18	2.55	36.39
S75	50	1.69-0.20	34	1.04	15.80	6.31	3.87	5.44	39.94
S75	10	1.66-0.20	170	5.21	15.80	6.87	8.79	108.05	43.48
W45	100	1.72-0.20	17	0.35	23.46	2.22	1.90	5.65	9.46
W60	100	1.74-0.20	17	0.26	31.07	1.80	1.72	7.32	5.79
W75	100	1.70-0.20	17	0.21	38.73	1.96	1.52	4.42	5.06

[a]Maximum value measured

Table 4-2. Electrical performance of microbatteries as a function of area and volume.

Battery Type	Load (kΩ)	Area (cm²)	Electrode Thickness (μm)	Areal Capacity (μAh/cm²)	Energy Density (μWh/cm²μm)	Power Density (μW/cm²μm)
WS30	100	0.1264	1.5	11.16	7.65	41.88
S45	100	0.1582	1.5	11.95	6.62	21.58
S60	100	0.1892	1.5	24.05	9.41	9.76
S75	100	0.2206	1.5	26.07	9.61	7.71
S75	50	0.2206	1.5	28.60	11.70	16.44
S75	10	0.2206	1.5	31.14	26.56	326.53
W45	100	0.1582	1.5	14.03	8.01	23.81
W60	100	0.19	1.5	9.47	6.04	25.68
W75	100	0.2218	1.5	8.84	4.57	13.29

Table 4-3. Capacity of microbatteries activated using physiological fluids.

Fluid	Battery type	Load (kΩ)	Voltage Range (V)	Load Current (μA)[a]	Current density (mA/cm²)[a]	Theoretical capacity (μAh)	Capacity (μAh)	Energy (μWh)	Power (μW)	η (%)
Urine	S45	50	0.80-0.20	16	0.49	15.80	7.04	4.65	8.41	44.56
Saliva	S45	50	0.80-0.20	16	0.49	15.80	5.13	2.87	5.31	32.47
Blood	S45	50	0.85-0.20	17	0.52	15.80	4.49	3.20	9.65	28.42
Blood	S60	10	0.75-0.20	75	2.30	15.80	6.82	4.09	33.35	43.16
Blood	S60	1	0.55-0.20	550	17.03	15.80	7.17	2.78	135.12	45.38

[a]Maximum value measured

Table 4-4. Electrical performance of microbatteries activated using physiological fluids as a function of area and volume.

Fluid	Battery Type	Load (kΩ)	Area (cm²)	Electrode Thickness (μm)	Areal Capacity (μAh/cm²)	Energy Density (μWh/cm²μm)	Power Density (μW/cm²μm)
Urine	S45	50	0.1582	1.5	44.50	19.60	35.44
Saliva	S45	50	0.1582	1.5	32.43	12.09	22.38
Blood	S45	50	0.1582	1.5	28.38	13.49	40.67
Blood	S60	10	0.1892	1.5	36.05	14.41	117.51
Blood	S60	1	0.1892	1.5	37.90	9.80	476.11

Microbattery Activated by Biofluids

The microbatteries were further tested using blood, urine, and saliva as the activation electrolyte (Table 4-3), which are 3 of the most commonly used physiological fluids in health screening. Figure 4-4 and 4-5 shows a plot of the experimental data obtained for the output voltage of microbattery S45 and S60. For these experiments, 8 μL of the target fluid were micropipetted to the surface of the battery. From Figure 4-5A, the maximum voltage output measured was 0.85 V when using blood as the activation fluid and 0.8 V when using saliva or urine as the activation fluid. A 50 kΩ resistor was used as the load in these experiments. When using urine as the electrolyte and taking 0.2 V as the cut-off voltage, the maximum discharge time obtained for the microbattery was close to 35 minutes. For blood and saliva, the discharge times where

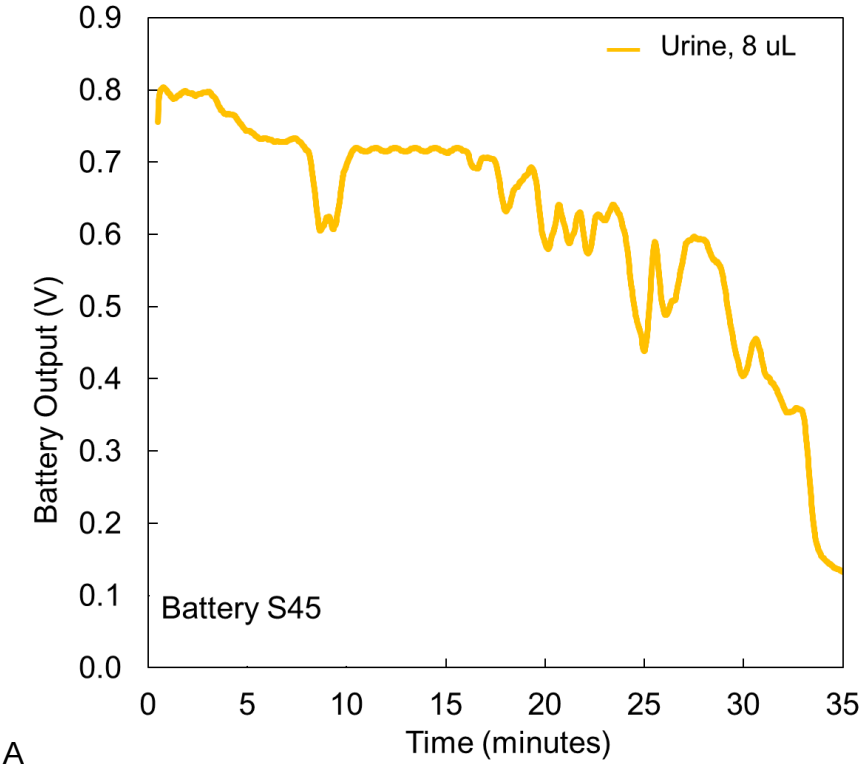

A

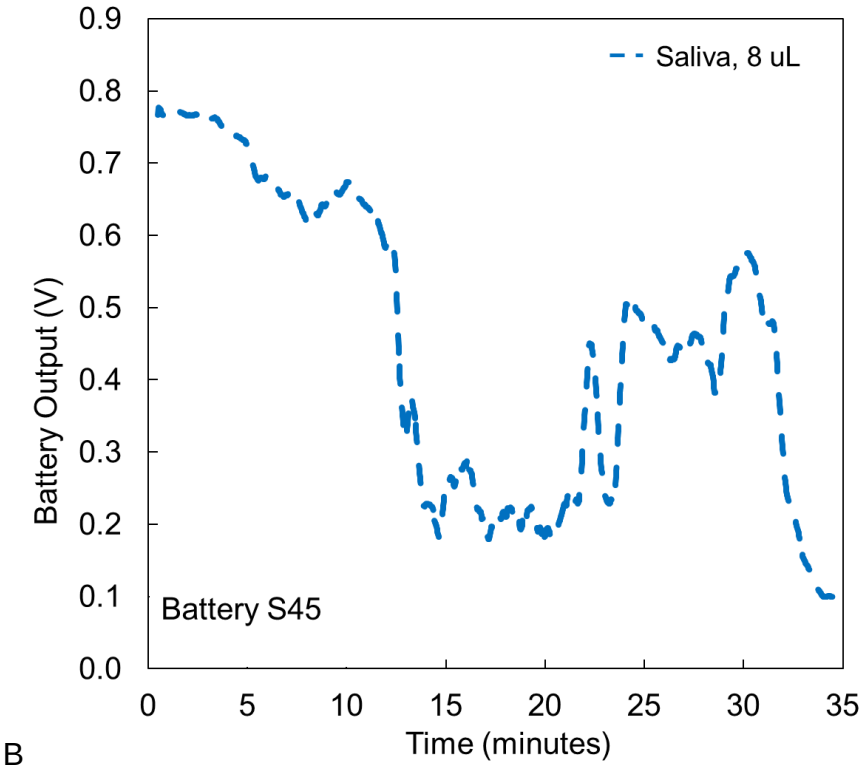

B

Figure 4-4. Voltage output for microbatteries activated using different electrolytes. A) Battery activated using urine. B) Battery activated suing saliva.

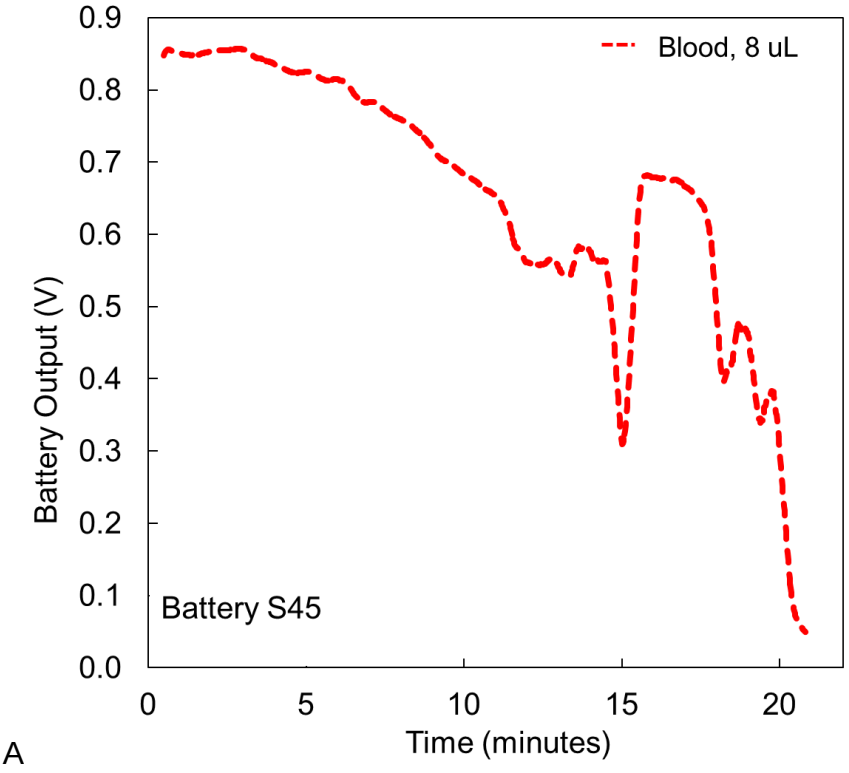

A

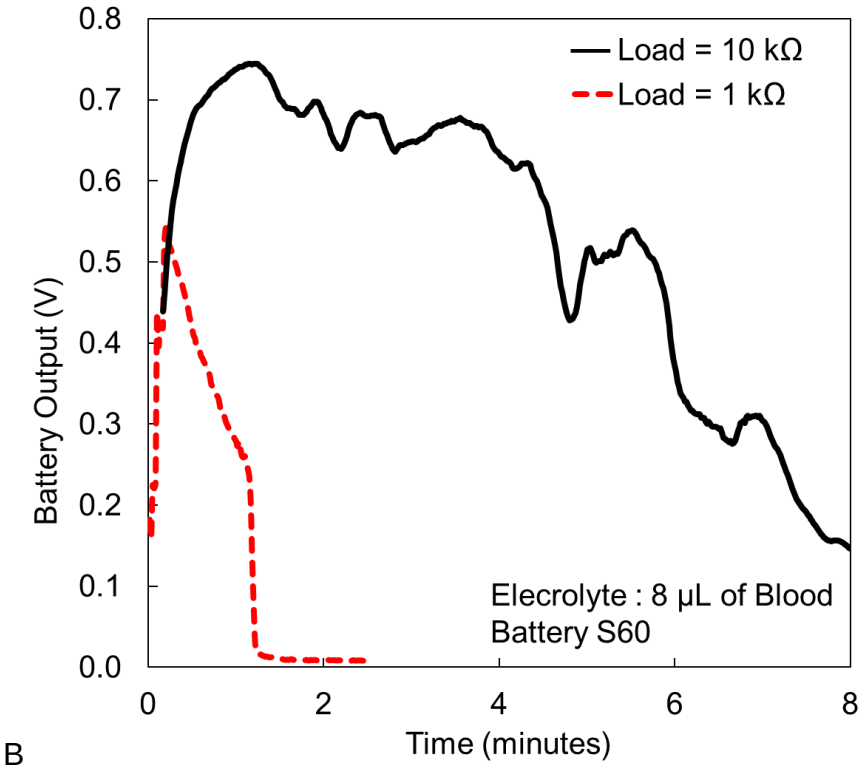

B

Figure 4-5. Voltage output for microbattery types S60 and S45 activated using blood. A) Output for S45 using 50 kΩ. B) Output for S60 using different loads.

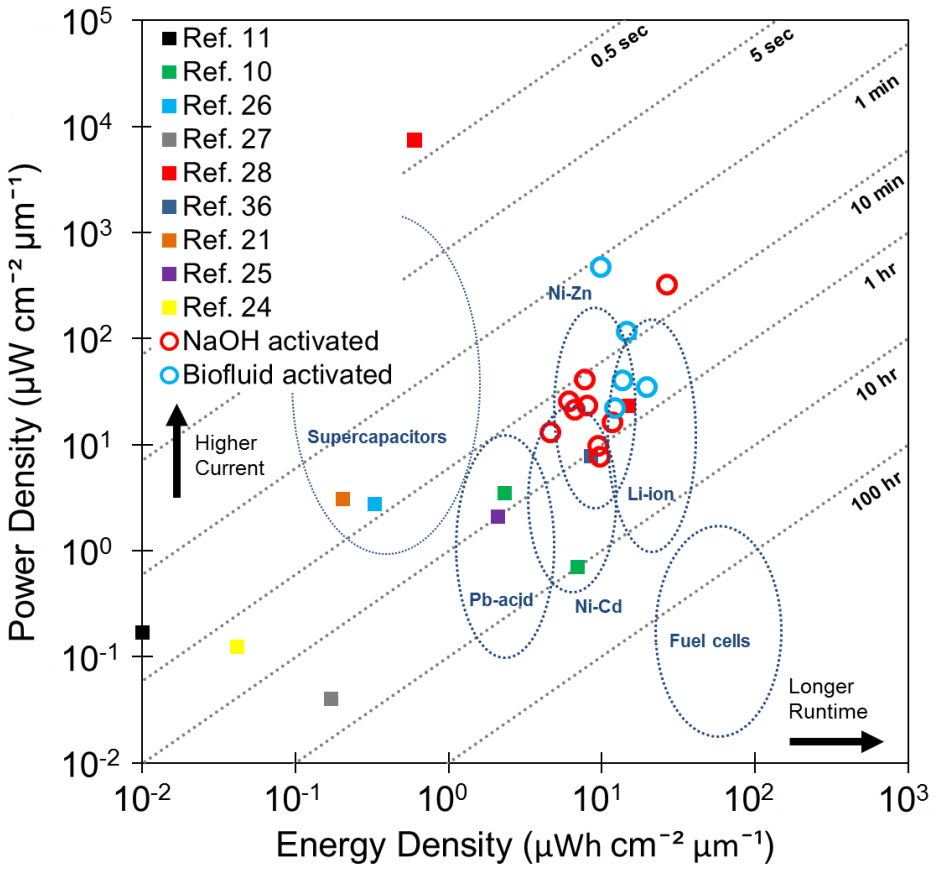

Figure 4-6. Ragone plot comparing the performance of our microbatteries with previously published batteries and commercial technologies.

close to 20 minutes. The maximum experimental capacity obtained was 7.17 µAh when using blood as the activation fluid. The smallest resistance value used in our experiments was 1kΩ, which translate into a maximum discharge current of 0.55 mA. For this case, the operating time of the battery was less than 2 minutes and the maximum output voltage was 0.55 V, as shown in Figure 4-5B. When using a load value of 1kΩ, the reaction kinetics of the microbattery was controlled not only by the electrochemical resistance but by the internal ohmic loses as well. Additionally, we observed that in the case of physiological fluids, the discharge time of the microbattery

Table 4-5. Performance comparison between our microbatteries and previously published microbatteries.

	Chemistry	Type	Electrode Thickness (μm)	Area (cm^2)	Flexible	Voltage Range (V)	Capacity (μAh)	Areal Capacity (μAh/cm^2)	Energy Density (μWh/cm^2μm)	Power Density (μW/cm^2μm)
S45	Al-AgO-Urine	On-demand	1.5	0.1582	Yes	0.8-0.2	7.04	44.50	19.59	35.44
S60	Al-AgO-Blood	On-demand	1.5	0.1892	Yes	0.6-0.2	7.17	37.90	9.80	476.11
S75	Al-AgO-NaOH	On-demand	1.5	0.2206	Yes	1.7-0.2	15.80	31.14	26.56	326.53
Ref. 11	Ni-Zn	Rechargeable	200	0.25	No	1.7-1.3	0.63	2.50	0.01	0.17
Ref. 10	MCMB-MoOS	Rechargeable	500	1.33	No	2.2-1.3	2660.00	2000.00	7.00	0.70
Ref. 10	MCMB-MoOS	Rechargeable	500	1.33	No	2.2-1.3	n/r	n/r	2.31	3.50
Ref. 26	Carbon-PPYDBS	Rechargeable	65	1	No	3.8-2.2	10.60	10.60	0.33	2.77
Ref. 27	LiCoO2-Li4Mn5O12	Rechargeable	180	27	No	1.2	864.00	32.00	0.17	0.04
Ref. 28	NiSn-LMO	Rechargeable	15	0.02	No	4.0-2.0	1.67	83.50	15.00	23.00
Ref. 28	NiSn-LMO	Rechargeable	12.6	0.017	No	4.0-2.0	0.05	3.02	0.60	7400.00
Ref. 36	AgO-Zn	Rechargeable	25	0.02	No	1.6-0.90	2.75	137.50	8.52	7.74
Ref. 21	Au-Zn-H2SO4	On-Demand	1000	0.01	No	0.9-0.1	3.66	366.00	0.20	3.05
Ref. 25	AgCl-Mg-Water	On-demand	20	1.44	No	1.6-0.4	1260.00	875.00	2.10	2.10
Ref. 22	Mg-CuCl-Urine	On-demand	7000	18	No	1.4-0.6	n/r	n/r	n/r	n/r
Ref. 24	Pt-Zn-Gastric fluid	On-demand	2000	1.2	No	0.7-0.1	190.00	158.33	0.04	0.13

was related to the time it took for the fluid to completely dry. Replenishing the activation fluid could help extend the theoretical capacity and discharge time of the microbatteries when using physiological fluids. Tabulated results of the electrical performance per unit volume are shown in Table 4-4.

Volumetric electrical performance of batteries at the microscale needs to be considered because of the inherent space constraint of biomedical microsystems. Over the past decade, researchers have focused on increasing the areal energy density of microbatteries rather than volumetric energy density by creating complex geometries with high aspect ratios. The results are microbatteries fabricated with complex methods that have an extremely low volumetric energy and power densities. Table 4-5 and Figure 4-6 present a comparison of the volumetric energy density and power density between our microbatteries and previously p microbatteries. The power density of our microbatteries is greater than the best published microbatteries except one, but unlike other published microbatteries, our batteries achieve a high volumetric power density without sacrificing energy density.

Conclusions

In response to the need for power sources that could be used in disposable, smart, and on demand electronic microsystems for the medical and biological fields, we have developed a unique microfabrication process using conventional MEMS techniques to fabricate a flexible microbattery. In this project, we designed, fabricated, and tested seven microbatteries having different footprint areas. The smallest microbattery measured 2.6 mm in length, 4.86 mm in width, and 8 μm in thickness. Aluminum was selected as the anode, silver oxide as the cathode, and polyimide as the flexible substrate. In this initial prototype, we have demonstrated that these

microbatteries can be activated with a wide range of physiological fluids, such as blood, urine, and saliva for on-demand operation. Voltage output measurements indicated that these microbatteries achieved a maximum output voltage of 1.75 V, capacity of 7.17 μAh, load current of 0.55 mA, and a maximum efficiency of 46%. We anticipate that the efficiency of the battery can be improved significantly by refreshing the activation fluid and using a load current that maximizes the capacity of the battery. Future studies will focus on improving battery efficiency and crating battery circuit models that will help in the design of application specific integrated circuits. Additional efforts will be directed towards developing viable methods for integrating our microbattery with CMOS integrated circuits in order to develop microsystems for biomedical applications.

LIST OF REFERENCES

[1] R. Dreslinski, M. Wieckowski, D. Blaauw, D. Sylvester, and T. Mudge, "Near-Threshold Computing: Reclaiming Moore's Law Through Energy Efficient Integrated Circuits," *Proceedings of the Ieee,* vol. 98, pp. 253-266, Feb 2010.

[2] R. Bashirullah, "Wireless Implants," *Ieee Microwave Magazine,* vol. 11, pp. S14-S23, Dec 2010.

[3] J. Rabaey, J. Ammer, B. Otis, E. Burghardt, Y. Chee, N. Pletcher*, et al.*, "Ultra-low-power design - The roadmap to disappearing electronics and ambient intelligence," *Ieee Circuits & Devices,* vol. 22, pp. 23-29, Jul 2006.

[4] M. Fojtik, D. Kim, G. Chen, Y. Lin, D. Fick, J. Park*, et al.*, "A Millimeter-Scale Energy-Autonomous Sensor System With Stacked Battery and Solar Cells," *Ieee Journal of Solid-State Circuits,* vol. 48, pp. 801-813, Mar 2013.

[5] H. Yu, G. Irby, D. Peterson, M. Nguyen, G. Flores, N. Euliano*, et al.*, "Printed capsule antenna for medication compliance monitoring," *Electronics Letters,* vol. 43, pp. 1179-1181, Oct 2007.

[6] H. Tao, M. Brenckle, M. Yang, J. Zhang, M. Liu, S. Siebert*, et al.*, "Silk-Based Conformal, Adhesive, Edible Food Sensors," *Advanced Materials,* vol. 24, pp. 1067-1072, Feb 2012.

[7] L. DiCarlo, "Role for direct electronic verification of pharmaceutical ingestion in pharmaceutical development," *Contemporary Clinical Trials,* vol. 33, pp. 593-600, Jul 2012.

[8] C. Chin, V. Linder, and S. Sia, "Commercialization of microfluidic point-of-care diagnostic devices," *Lab on a Chip,* vol. 12, pp. 2118-2134, 2012.

[9] G. Teixidor, R. Zaouk, B. Park, and M. Madou, "Fabrication and characterization of three-dimensional carbon electrodes for lithium-ion batteries," *Journal of Power Sources,* vol. 183, pp. 730-740, Sep 2008.

[10] M. Nathan, D. Golodnitsky, V. Yufit, E. Strauss, T. Ripenbein, I. Shechtman*, et al.*, "Three-dimensional thin-film Li-ion microbatteries for autonomous MEMS," *Journal of Microelectromechanical Systems,* vol. 14, pp. 879-885, Oct 2005.

[11] F. Chamran, Y. Yeh, H. Min, B. Dunn, and C. Kim, "Fabrication of high-aspect-ratio electrode arrays for three-dimensional microbatteries," *Journal of Microelectromechanical Systems,* vol. 16, pp. 844-852, Aug 2007.

[12] V. Lifton, S. Simon, J. Holmqvist, T. Ebefors, D. Jansson, and N. Svedin, "Design and Fabrication of Addressable Microfluidic Energy Storage MEMS Device," *Journal of Microelectromechanical Systems,* vol. 21, pp. 1392-1401, Dec 2012.

[13] A. Cardenas-Valencia, C. Biver, and L. Langebrake, "Reserve, thin form-factor, hypochlorite-based cells for powering portable systems: Manufacture (including MEMS processes), performance and characterization," *Journal of Power Sources,* vol. 166, pp. 273-283, Mar 2007.

[14] P. Humble, J. Harb, and R. LaFollette, "Microscopic nickel-zinc batteries for use in autonomous microsystems," *Journal of the Electrochemical Society,* vol. 148, pp. A1357-A1361, Dec 2001.

[15] C. Ho, J. Evans, and P. Wright, "Direct write dispenser printing of a zinc microbattery with an ionic liquid gel electrolyte," *Journal of Micromechanics and Microengineering,* vol. 20, Oct 2010.

[16] C. Ho, K. Murata, D. Steingart, J. Evans, and P. Wright, "A super ink jet printed zinc-silver 3D microbattery," *Journal of Micromechanics and Microengineering,* vol. 19, Sep 2009.

[17] K. Braam, S. Volkman, and V. Subramanian, "Characterization and optimization of a printed, primary silver-zinc battery," *Journal of Power Sources,* vol. 199, pp. 367-372, Feb 2012.

[18] A. Armutlulu, Y. Fang, S. Kim, C. Ji, S. Allen, and M. Allen, "A MEMS-enabled 3D zinc-air microbattery with improved discharge characteristics based on a multilayer metallic substructure," *Journal of Micromechanics and Microengineering,* vol. 21, Oct 2011.

[19] J. Song, X. Yang, S. Zeng, M. Cai, L. Zhang, Q. Dong*, et al.*, "Solid-state microscale lithium batteries prepared with microfabrication processes," *Journal of Micromechanics and Microengineering,* vol. 19, Apr 2009.

[20] W. West, J. Whitacre, V. White, and B. Ratnakumar, "Fabrication and testing of all solid-state microscale lithium batteries for microspacecraft applications," *Journal of Micromechanics and Microengineering,* vol. 12, pp. 58-62, Jan 2002.

[21] K. Lee and L. Lin, "Electrolyte-based on-demand and disposable microbattery," *Journal of Microelectromechanical Systems,* vol. 12, pp. 840-847, Dec 2003.

[22] K. Lee, "Urine-activated paper batteries for biosystems," *Journal of Micromechanics and Microengineering,* vol. 15, pp. S210-S214, Sep 2005.

[23] K. Lee, "Two-step activation of paper batteries for high power generation: design and fabrication of biofluid- and water-activated paper batteries," *Journal of Micromechanics and Microengineering,* vol. 16, pp. 2312-2317, Nov 2006.

[24] H. Jimbo and N. Miki, "Gastric-fluid-utilizing micro battery for micro medical devices," *Sensors and Actuators B-Chemical,* vol. 134, pp. 219-224, Aug 2008.

[25] F. Sammoura, K. Lee, and L. Lin, "Water-activated disposable and long shelf life microbatteries," *Sensors and Actuators a-Physical,* vol. 111, pp. 79-86, Mar 2004.

[26] H. S. Min, B. Y. Park, L. Taherabadi, C. L. Wang, Y. Yeh, R. Zaouk*, et al.*, "Fabrication and properties of a carbon/polypyrrole three-dimensional microbattery," *Journal of Power Sources,* vol. 178, pp. 795-800, Apr 2008.

[27] M. Kotobuki, Y. Suzuki, H. Munakata, K. Kanamura, Y. Sato, K. Yamamoto*, et al.*, "Effect of sol composition on solid electrode/solid electrolyte interface for all-solid-state lithium ion battery," *Electrochimica Acta,* vol. 56, pp. 1023-1029, Jan 2011.

[28] J. H. Pikul, H. G. Zhang, J. Cho, P. V. Braun, and W. P. King, "High-power lithium ion microbatteries from interdigitated three-dimensional bicontinuous nanoporous electrodes," *Nature Communications,* vol. 4, Apr 2013.

[29] H. Kim, R. Auyeung, and A. Pique, "Laser-printed thick-film electrodes for solid-state rechargeable Li-ion microbatteries," *Journal of Power Sources,* vol. 165, pp. 413-419, Feb 2007.

[30] S. D. Senturia, *Microsystem design*. Boston: Kluwer Academic Publishers, 2001.

[31] Q. Li and N. Bjerrum, "Aluminum as anode for energy storage and conversion: a review," *Journal of Power Sources,* vol. 110, pp. 1-10, Jul 2002.

[32] H. Liu, X. Xia, and Z. Guo, "A novel silver oxide electrode and its charge-discharge performance," *Journal of Applied Electrochemistry,* vol. 32, pp. 275-279, Mar 2002.

[33] X. Jin and J. Lu, "The potential valleys of silver oxide electrodes during pulse discharge," *Journal of Power Sources,* vol. 104, pp. 253-259, Feb 2002.

[34] T. B. Reddy and D. Linden, *Linden's handbook of batteries*, 4th ed. New York: McGraw-Hill, 2011.

[35] S. Pal and H. Xie, "Fabrication of robust electrothermal MEMS devices using aluminum-tungsten bimorphs and polyimide thermal isolation," *Journal of Micromechanics and Microengineering,* vol. 22, Nov 2012.

[36] F. Albano, Y. Lin, D. Blaauw, D. Sylvester, K. Wise, and A. Sastry, "A fully integrated microbattery for an implantable microelectromechanical system," *Journal of Power Sources,* vol. 185, pp. 1524-1532, Dec 2008.

BIOGRAPHICAL SKETCH

Edgar Felipe Garay was born in Cabimas, Venezuela, in 1982. He received the B.S. degree in physics, in 2009, and the B.S. degree in electrical engineering, in 2010, from Florida International University, Miami, FL, and the M.S. degree in electrical engineering from University of Florida, Gainesville, FL, in 2013. He is currently pursuing the Ph.D. degree in electrical engineering at University of Florida, Gainesville.

Since 2011 he has been a research assistant at the Integrated Circuits Laboratory under the supervision of Dr. Rizwan Bashirullah. His research interest includes the fabrication of microelectromechanical systems, integrated circuit design, and their biomedical applications.

Mr. Garay was awarded the Latin American Fellowship award, the Ronald E. McNair Scholars Award of Excellence, and the South East Alliance for Graduate Education and the Professoriate (SEAGEP) research award.